

## Direct Measurement of the Negative-Kaon Form Factor

E. B. Dally,<sup>(a)</sup> J. M. Hauptman, J. Kubic, D. H. Stork, and A. B. Watson  
*Physics Department, University of California, Los Angeles, California 90024*

and

Z. Guzik, T. S. Nigmanov, V. D. Riabtsov, E. N. Tsyganov, and A. S. Vodopianov  
*Joint Institute for Nuclear Research, Dubna, U. S. S. R.*

and

A. Beretvas,<sup>(b)</sup> A. Grigorian,<sup>(c)</sup> J. C. Tompkins,<sup>(d)</sup> T. E. Toohig, and A. A. Wehmann  
*Fermi National Accelerator Laboratory, Batavia, Illinois 60510*

and

J. A. Poirier, C. A. Rey,<sup>(e)</sup> and J. T. Volk<sup>(f)</sup>  
*Physics Department, University of Notre Dame, Notre Dame, Indiana 46556*

and

P. D. Rapp<sup>(g)</sup> and P. F. Shepard  
*Physics Department, University of Pittsburgh, Pittsburgh, Pennsylvania 15620*

(Received 17 March 1980)

The electromagnetic form factor of the negative kaon has been measured by direct scattering of 250-GeV/c kaons from the stationary electrons of a liquid-hydrogen target. The deviation of the measured elastic scattering cross section from the point cross section may be characterized by a root-mean-square kaon radius of  $\langle r_{K^-}^2 \rangle^{1/2} = 0.53 \pm 0.05$  fm.

PACS numbers: 14.40.Fw, 13.40.Fn, 13.85.Dz

A first measurement of the negative-kaon electromagnetic form factor has been obtained by elastically scattering 250-GeV/c kaons from electrons in a liquid-hydrogen target. The departure of the elastic scattering cross section from the point (pt) cross section is given by

$$d\sigma/dq^2 = (d\sigma/dq^2)_{\text{pt}} |F_K(q^2)|^2,$$

where  $F_K(q^2)$  is the kaon form factor. The maximum kinematically allowed recoil electron energy is 128 GeV, corresponding to  $q^2 = 0.131$  (GeV/c)<sup>2</sup>. The beam kaon and the scattered kaon and electron were detected with a high-resolution single-arm spectrometer. Geometric efficiency was high (84% to 100%) for electron energies from 36 to 116 GeV, and in this paper we present data on the kaon form factor over the corresponding momentum-transfer interval  $0.037 \leq q^2 \leq 0.119$  (GeV/c)<sup>2</sup>.

Elastic scatters were recorded by the apparatus illustrated in Fig. 1. The incident-beam kaon and the scattered kaon and electron were tracked by both proportional wire chamber (PWC) stations and by drift chamber (DC) stations. Both chamber types were used in track finding and event reconstruction to provide the high redun-

dancy required for good efficiency. With PWC calibration an overall drift chamber resolution of approximately 100  $\mu\text{m}$  was achieved and it made possible good discrimination against the copious strong-interaction background. The momentum of the scattered kaon and of the electron were determined by two magnets with a total field integral of 70.35 kg-m followed by three PWC stations. Located behind the last PWC station was a lead-glass shower-counter system 21 radiation lengths in thickness which was used in the trigger and in the final background determination.

An event trigger was determined by stringent beam requirements and a loose two-particle requirement. The beam logic was

$$\text{BEAM} \equiv C_D B_0 B_1 B_2 \cdot \overline{B_{2\text{TWO}}} \cdot \overline{\text{AH}} \cdot \text{KILL} \\ \cdot \text{SP} \cdot \overline{\text{DP}} \cdot \text{DCD}.$$

$C_D$  represents the differential-Čerenkov-counter signal requirement (100 ft of helium at  $\sim 13$  psi provided unambiguous identification of the 2% kaons in the beam).  $B_0$ ,  $B_1$ , and  $B_2$  represent beam scintillation-counter signals.  $B_{2\text{TWO}}$  is an additional signal from the counter  $B_2$  with the dis-

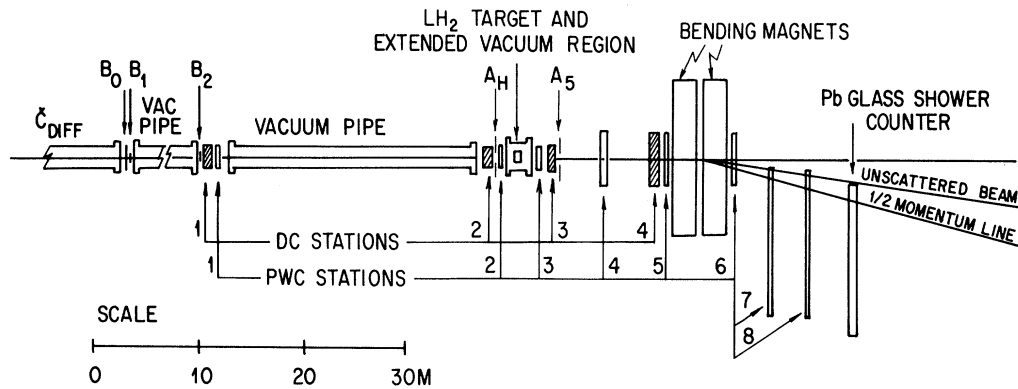


FIG. 1. Arrangement of the spectrometer apparatus. While transverse dimensions are not drawn to scale, they are magnified approximately by a factor of 10 over longitudinal dimensions.  $B_0$ ,  $B_1$ ,  $B_2$ ,  $A_H$ , and  $A_5$  are scintillation counters. Each PWC station has four planes. Stations 1–6 have transverse readout coordinate pairs with station 4 rotated to  $45^\circ$ . Stations 7 and 8 each have two  $x$  planes and two planes rotated to  $\pm 29^\circ$ . The four drift chamber stations have four  $x$  planes and four  $y$  planes each. Helium bags between drift chamber and PWC stations are not shown.

crimination level set to twice minimum ionization. A beam halo counter AH defined the transverse dimensions of the beam. KILL required that no other beam particle preceded the event within 500 ns nor followed it within 60 ns. The beam PWC's provided a single-particle requirement SP and discriminated against double particles DP. Similar requirements were formed by the beam drift chambers in the logic decision DCD. For a two-sec beam spill, the typical number of beam kaons was 18 000 (out of  $10^6$  beam particles). Of these, about 6000 satisfied the clean beam-trigger requirement. The event trigger was

$$\text{EVENT} \equiv \text{BEAM} \cdot \overline{A_5} \cdot \text{TP} \cdot C,$$

where  $A_5$  was a scintillation counter with a circular hole 10.16 cm in diameter which vetoed some of the strong-interaction events (a small correction was required for elastic kaon-electron events vetoed because of radiative photons and  $\delta$  rays striking the  $A_5$  scintillator). TP required that there were at least two particles in PWC stations 5 and 6. Requirement C was that some combination of the five lead-glass shower-counter sections produced a pulse consistent with an electron from an elastic kaon-electron scattering. The trigger rate was about  $10^{-3}$  per incident kaon or 10 per spill. Less than 1% of these were elastic scattering events.

Events were reconstructed by finding and fitting horizontal and vertical track projections and then matching these projections with rotated

PWC's in stations 4, 7, or 8. Pairs of secondary tracks having a common target origin with an incident beam track were taken to be candidates for elastic scattering. The target vacuum windows were 1 m from either end of the liquid-hydrogen flask, allowing clean identification of events originating in the target flask. The inefficiency in the event-finding procedures was estimated from detailed studies of the analysis programs and by Monte Carlo calculations with use of real chamber efficiencies.

Events were tested for energy and momentum conservation in the elastic scattering process by means of a  $\chi^2$  fit. In this fit it was assumed that an undetected photon was produced in the electron's direction either by radiation accompanying the elastic scattering or by electron bremsstrahlung in the target or spectrometer material. Events were selected to have  $\chi^2$  less than 30 and to have radiated photon energy less than 12 GeV. Losses due to the  $\chi^2$  and photon-energy cuts were determined by Monte Carlo calculations.

The electron energies measured in the lead-glass shower-counter system had a resolution function with typical standard deviation of 3.1%. A cut was made requiring the pulse height to be greater than 80% of that expected from the momentum measurement of the electron. The small hadronic background which survived various cuts was determined by extrapolating the measured hadronic-background pulse-height distribution under the electron peak.

Table I lists the corrections applied to the da-

TABLE I. Corrections to the data.

Effect	Correction (%)
<i>q</i> <sup>2</sup> -independent corrections	
Beam-momentum cut	0.5 ± 0.1
<i>e</i> , <i>μ</i> , <i>π</i> , and <i>p̄</i> contaminations	0.1 ± 0.2
Primary <i>K</i> decay	1.5 ± 0.1
Primary <i>K</i> attenuation	2.9 ± 0.1
Target electron density	0.0 ± 0.3
Secondary <i>K</i> attenuation	4.1 ± 0.1
δ rays in <i>A</i> <sub>5</sub>	0.4 ± 0.1
Trigger inefficiencies	0.2 ± 0.2
Range of <i>q</i> <sup>2</sup> -dependent corrections	
Geometric inefficiency	(0.0 - 13.1) ± (0.0 - 0.4)
Radiative corrections <sup>a</sup>	(4.1 - 10.5) ± (0.2 - 0.3)
Secondary <i>K</i> decay	(1.4 - 2.1) ± (0.1 - 0.1)
Hadronic background	(0.0 - 1.7) ± (0.0 - 1.2)
Track-finding inefficiency	(2.7 - 4.0) ± (0.5 - 0.6)
External bremsstrahlung	(13.9 - 25.6) ± (0.2 - 0.3)

<sup>a</sup>Ref. 1.

ta. The resulting form factor is shown as a function of *q*<sup>2</sup> in Table II and in Fig. 2. The errors shown are the combined statistical and systematic errors.

A fit to the form factor with the pole form  $|F_K(q^2)|^2 = (1 + \frac{1}{8} q^2 \langle r_K^2 \rangle)^{-2}$  results in  $\langle r_K^2 \rangle = 0.28 \pm 0.05 \text{ fm}^2$ , or  $\langle r_K^2 \rangle^{1/2} = 0.53 \pm 0.05 \text{ fm}$  and is shown as the solid curve in Fig. 2. The error is dominated by the statistics of the data sample but accurate normalization and the constraint of unit form factor at *q*<sup>2</sup> = 0 are required. If the normalization uncertainty (determined by combining the errors of Table I in quadrature) were *tripled*, the fit would yield  $\langle r_K^2 \rangle^{1/2} = 0.54 \pm 0.07 \text{ fm}$ . An *unnormalized* fit yields  $\langle r_K^2 \rangle^{1/2} = 0.65 \pm 0.15 \text{ fm}$  and is

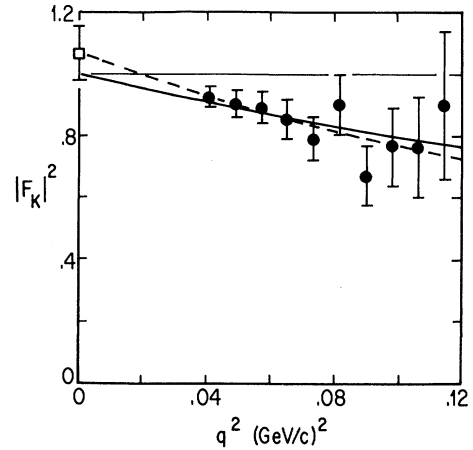


FIG. 2. Kaon form factor. The pole fit, constrained to a value of 1 at *q*<sup>2</sup> = 0, is shown as the solid curve. An unnormalized fit is shown as the dashed curve with the fitted value  $1.07 \pm 0.09$  indicated at *q*<sup>2</sup> = 0.

shown by the dashed curve in Fig. 2 (the error bar at *q*<sup>2</sup> = 0 corresponds to the fitted value  $|F(0)|^2 = 1.07 \pm 0.09$ ). Use of the dipole form  $|F_K(q^2)|^2 = (1 + \frac{1}{12} q^2 \langle r_K^2 \rangle)^{-4}$  gives negligible difference in the fit. The result was also found to be insensitive to change in the cuts in the radiated photon energy, in the  $\chi^2$ , and in the geometry. The result may be compared to  $\langle r_\pi^2 \rangle = 0.31 \pm 0.04 \text{ fm}^2$ , or  $\langle r_\pi^2 \rangle^{1/2} = 0.56 \pm 0.04 \text{ fm}$  for the pion.<sup>2</sup>

An accurate theoretical prediction has not been produced, but it is of interest to compare our result for the electromagnetic form factor with the Chou-Yang model in which the kaon hadronic form factor is extracted from hadronic scattering data. The model gives<sup>3</sup>  $\langle r_K^2 \rangle^{1/2} = 0.54 \pm 0.14 \text{ fm}$ . Greenberg, Nussinov, and Sucher<sup>4</sup> suggest a relativistically valid quark-model inequality

TABLE II. Events, measured cross section, and form factor versus *q*<sup>2</sup>.

<i>q</i> <sup>2</sup> [(GeV/c) <sup>2</sup> ]	Number of events	Events after correction	<i>dσ/dq</i> <sup>2</sup> [ $\mu\text{b (GeV/c)}^{-2}$ ]	$ F_K ^2$
0.0409	728	1020	100.6 ± 3.8	0.93 ± 0.03
0.0491	459	625	61.7 ± 2.9	0.90 ± 0.04
0.0572	295	407	40.2 ± 2.4	0.89 ± 0.05
0.0654	190	267	26.2 ± 1.9	0.85 ± 0.06
0.0736	120	171	16.7 ± 1.5	0.79 ± 0.07
0.0818	94	137	13.2 ± 1.4	0.90 ± 0.09
0.0899	48	70	6.8 ± 1.0	0.67 ± 0.10
0.0981	37	55	5.2 ± 0.9	0.77 ± 0.13
0.1063	23	36	3.3 ± 0.7	0.76 ± 0.16
0.1145	15	26	2.2 ± 0.6	0.90 ± 0.23

which relates the ratio of strange ( $m_s$ ) to non-strange ( $m_n$ ) quark masses to the ratio of electromagnetic radii for neutral and charged kaons. Combining the recently measured<sup>5</sup> neutral-kaon radius  $\langle r_{K^0} \rangle = -0.054 \pm 0.026 \text{ fm}^2$  with the present charged-kaon radius measurement, we find  $m_s/m_n \geq 1.39 \pm 0.28$ .

In conclusion, our best determination of the negative-kaon radius is  $\langle r_{K^-} \rangle^{1/2} = 0.53 \pm 0.05 \text{ fm}$  as obtained from the fit to the directly measured form factor constrained to unity at zero momentum transfer.

We wish to express our gratitude to Professor R. R. Wilson for his support of this form factor experiment and to thank the Fermilab staff whose assistance made possible the success of this experiment. This work was supported in part by the U. S. Department of Energy and by the U. S. National Science Foundation.

<sup>(a)</sup>Now at Varian Associates, Hansen Way, Palo Alto, Cal. 94306.

<sup>(b)</sup>Now at Rutgers University, Piscataway, N.J. 08854.

<sup>(c)</sup>Now at Hughes Aircraft Co., Culver City, Cal. 90230.

<sup>(d)</sup>High Energy Physics Laboratory, Stanford University, Stanford, Cal. 94305.

<sup>(e)</sup>Now at Interasonics, Inc., Northbrook, Ill. 60062.

<sup>(f)</sup>Now at Ohio State University, Columbus, Ohio 43210.

<sup>(g)</sup>Now at Fermi National Accelerator Laboratory, Batavia, Ill. 60510.

<sup>1</sup>D. Yu. Bardin, G. W. Micelmacher, and N. M. Shumaiko, Joint Institute for Nuclear Research Report No. E2-6235, 1972 (unpublished).

<sup>2</sup>E. Dally *et al.*, Phys. Rev. Lett. **39**, 1176 (1977).

<sup>3</sup>T. T. Chou, Phys. Rev. D **19**, 3327 (1979).

<sup>4</sup>O. W. Greenberg, S. Nussinov, and J. Sucher, Phys. Lett. **70B**, 465 (1977).

<sup>5</sup>W. R. Molzon *et al.*, Phys. Rev. Lett. **41**, 1213 (1978).

## Do Quarks Interact Pairwise and Satisfy the Color Hypothesis?

D. P. Stanley and D. Robsen

*Department of Physics, Florida State University, Tallahassee, Florida 32306*

(Received 29 April 1980)

A simple three-quark Hamiltonian based on a quark-antiquark interaction which accurately describes all  $q\bar{q}$  mesons has been solved numerically. Good agreement with the ground-state baryon mass spectrum is obtained if the  $qq$  and  $q\bar{q}$  interactions differ by an overall factor of 2 as expected from an octet color-exchange mechanism. The interactions in a three-quark system appear to be very well described by only a sum of pair interactions.

PACS numbers: 14.80.Dq, 12.40.Cc, 12.70.+q

One of the major differences between quantum electrodynamics (QED) and quantum chromodynamics (QCD) is the nature of the interaction between the field quanta. In QCD the field quanta (colored gluons) interact whereas in QED the photons do not interact. This difference is a consequence of the non-Abelian gauge transformations postulated for QCD which are specifically phrased in terms of the SU(3) color group. The major consequences of the color hypothesis for strong interactions between quarks are the following:

(1) At small distances one-gluon exchange<sup>1</sup> between a pair of quarks ( $i, j$ ) yields a Coulomb-like interaction with an overall strength which depends on color via the product  $\vec{F}_i \cdot \vec{F}_j$ , where the eight components of  $\vec{F}$  are the generators of SU(3) in color space. As the distance between quarks is decreased the effective coupling constant ap-

proaches zero corresponding to the concept of asymptotic freedom.

(2) At large distances the interaction between quarks is expected to lead to confinement, although as yet there is no rigorous derivation of this hypothesis (infrared slavery). Most recent work assumes that the interaction between quarks at large separations can be approximated by a string,<sup>2</sup> a boundary condition (bag models<sup>3</sup>), or a linear potential with an overall strength again depending on  $\vec{F}_i \cdot \vec{F}_j$ .

(3) For more than two quarks the possibility of genuine multibody interactions occurs because of the allowed multigluon vertices. At small distances a three-gluon vertex with each gluon being emitted or absorbed from a different quark is envisaged as a source of a three-body interaction. At larger distances one might also expect multi-